Capillary-lubrication force between rotating cylinders separated by a fluid interface

Aditya Jha,[1] Yacine Amarouchene,[1] and Thomas Salez[1, *]

[1] *Univ. Bordeaux, CNRS, LOMA, UMR 5798, F-33405 Talence, France.*

Two cylinders rotating next to each other generate a large hydrodynamic force if the intermediate space is filled with a viscous fluid. Herein, we explore the case where the cylinders are separated by two layers of viscous immiscible fluids, in the limit of small capillary deformation of the fluid interface. As the interface deformation breaks the system's symmetry, a novel force characteristic of soft lubrication is generated. We calculate this capillary-lubrication force, which is split into velocity-dependant and acceleration-dependant contributions. Furthermore, we analyze the variations induced by modifying the viscosity ratio between the two fluid layers, their thickness ratio, and the Bond number. Unlike standard elastic cases, where a repelling soft-lubrication lift force has been abundantly reported, the current fluid bilayer setting can also exhibit an attractive force due to the non-monotonic deflection of the fluid interface when varying the sublayer thickness. Besides, at high Bond numbers, the system's response becomes analogous to the one of a Winkler-like substrate with a viscous flow inside.

Keywords: low-Reynolds-number flows, lubrication theory, capillarity, fluid interfaces, fluid-structure interactions, contact mechanics.

I. INTRODUCTION

The movement of solid objects in viscous fluids has been the subject of detailed research in fluid sciences for more than a century [1, 2]. As opposed to particle motion in a bulk fluid [3–6], when an object moves in close proximity to a boundary, the resulting pressure field and the force exerted on the object are modified [7–10]. Such lubricated contacts have implications spanning over different domains, from tribology [11] to biomechanics of synovial fluids in joints [12, 13] or the transport of cells in the blood [14]. The understanding of single particle dynamics then further helps explaining the properties of clusters and suspensions [15–19].

Over the past decades, dedicated research has explored the influence of soft boundaries on the motion of the particles to understand the role of boundary elasticity on hydrodynamic flow. The force and torque felt by the particle approaching the boundary have been calculated [20, 21] and have been used to design the contactless rheological probes employed for soft materials [22, 23]. Surprisingly, as opposed to rigid boundaries, particles translating parallel to soft boundaries feel a repulsive lift force that arises out of the symmetry breaking induced by the elasticity of the wall [24–40]. The scope has been further expanded to explore the influence of fluid compressibility [41], fluid inertia [42], viscoelasticity of the boundary [34], and the inhomogeneities in slippage at the boundary [43].

As the solids become softer, capillary stresses dominate over the material's bulk elasticity, and inner flows become increasingly important. The latter start to modify the force and torque generated. In the limit of point forces, previous research [44, 45] has highlighted the pumping flow that can be observed when the interface deflection is accounted for. On the other hand, Leal and coworkers calculated the force felt by a finite-sized sphere moving near a fluid interface, by utilizing Lorentz's Reciprocal Theorem, for the regime of a large gap as compared to the size of the sphere [46–49]. Further developments included advancements in slender-body theory [50] to explain the swimming of microorganisms near fluid interfaces [51, 52], as well as the formation of floating biofilms [53]. A recent study on viscoelastic fluid substrates [54] also highlighted that capillary interfaces could result in an attractive force instead of a repulsive lift one.

While previous research has shown the importance and applicability of understanding the motion near a fluid interface, the characterization across different viscosity ratios and arbitrary layer thicknesses, for immiscible fluids, remains to be done. In the present article, we study the system of two rotating cylinders in close proximity to each other, separated by two viscous fluid layers. We calculate the force generated on one of the cylinders in the limit of small deformation of the fluid interface, as characterized by the capillary compliance. The article is organized as follows. We start by describing the viscocapillary lubrication problem at stake, followed by the theoretical methodology to obtain the different fields using perturbation analysis at small capillary compliance. We then discuss the implications of the deformable interface and the sub-layer flows on the force generated on the cylinder.

II. CAPILLARY-LUBRICATION THEORY

We consider two rigid infinite cylinders of radii a_1 and a_2 rotating with prescribed time-dependent angular velocities ω_1 and ω_2 near a fluid interface, as shown in Fig. 1. The interface is characterized by its surface tension σ, and separates two incompressible Newtonian viscous fluids, with dynamic shear viscosities η_1 and η_2, as well as mass densities ρ_1 and ρ_2 (with $\rho_2 < \rho_1$). The acceleration of gravity is denoted g. The thickness profiles $z = -h_1(x)$ and $z = h_2(x)$ of the bottom and top cylinders, depend on the horizontal position x. We denote by z the vertical position and by t the time.

A. Governing equations

We neglect fluid inertia and assume the typical thicknesses d_i, of the two fluids indexed by $i = 1, 2$, to be much smaller than the relevant horizontal length scales, defined by the hydrodynamic radii $\sqrt{2a_i d_i}$ [20], allowing us to invoke lubrication theory [55, 56]. Introducing the excess pressure fields $p_i(x, z, t)$ with respect to the hydrostatic contributions, and the horizontal velocity fields $u_i(x, z, t)$, the incompressible Stokes equations thus read at leading lubrication order:

$$\frac{\partial p_i}{\partial z} = 0 \ , \tag{1}$$

$$\frac{\partial p_i}{\partial x} = \eta_i \frac{\partial^2 u_i}{\partial z^2} \ . \tag{2}$$

In the near-contact region, in the limit of small gap, the shapes of the cylinders can be approximated by their
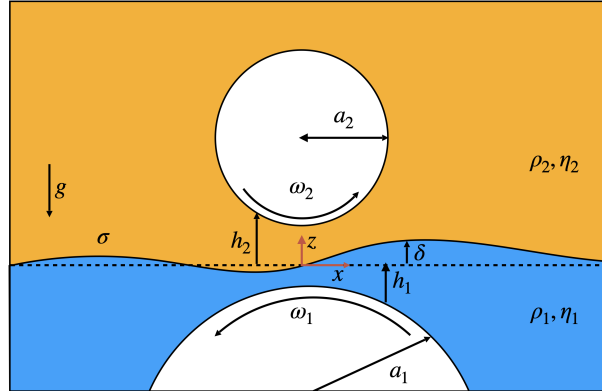

FIG. 1: Schematic of the system. Two rigid infinite cylinders rotate with prescribed velocities near a capillary interface between two incompressible Newtonian viscous fluids. The origin of spatial coordinates is located at the undeformed fluid interface ($z = 0$) in the line joining the centers of mass of the cylinders ($x = 0$). The deformed fluid interface is located at $z = \delta(x, t)$.

parabolic expansions, as:

$$h_1(x) \simeq d_1 + \frac{x^2}{2a_1} \ , \tag{3}$$

and:

$$h_2(x) \simeq d_2 + \frac{x^2}{2a_2} \ . \tag{4}$$

Finally, we close the equations by setting the flow boundary conditions. We impose no slip at the three interfaces alongside the balance of tangential and normal stresses at the fluid interface located at $z = \delta(x, t)$. Hence, at $z = -h_1$, one has:

$$u_1 = -\omega_1 a_1 \ , \tag{5}$$

at $z = h_2$, one has:

$$u_2 = \omega_2 a_2 \, , \tag{6}$$

and at $z = \delta$, one has:

$$u_2 = u_1, \tag{7}$$

$$\eta_2 \frac{\partial u_2}{\partial z} = \eta_1 \frac{\partial u_1}{\partial z} \, , \tag{8}$$

$$p_2 - p_1 \simeq \sigma \frac{\partial^2 \delta}{\partial x^2} + g\delta(\rho_2 - \rho_1) \, . \tag{9}$$

Let us now non-dimensionalize the equations through:

$$h_1(x) = d_2 H_1(X) \, , \qquad h_2(x) = d_2 H_2(X) \, , \qquad x = lX \, , \qquad z = d_2 Z \, ,$$

$$t = \frac{l}{c} T \, , \qquad u_1(x, z, t) = cU_1(X, Z, T) \, , \qquad u_2(x, z, t) = cU_2(X, Z, T) \, ,$$

$$p_1(x, t) = \frac{\eta_2 cl}{d_2^2} P_1(X, T) \, , \qquad p_2(x, t) = \frac{\eta_2 cl}{d_2^2} P_2(X, T) \, , \qquad \delta(x, t) = d_2 \Delta(X, T) \, ,$$

with the upper hydrodynamic radius $l = \sqrt{2a_2 d_2}$, and where c represents a characteristic horizontal velocity scale, e.g. $a_2\omega_2$. Moreover, the viscosity ratio is denoted by $M = \eta_1/\eta_2$. Using these dimensionless variables, Eqs. (3,4) become:

$$H_1(X) = \alpha + \frac{X^2}{\beta} \, , \tag{10}$$

$$H_2(X) = 1 + X^2 \, , \tag{11}$$

where $\alpha = d_1/d_2$ and $\beta = a_1/a_2$ are the geometrical aspect ratios of the problem. The solutions of the dimensionless versions of Eqs. (1,2) are of the form:

$$U_1 = \frac{P_1' Z^2}{2M} + C_1 Z + C_2 \, , \tag{12}$$

$$U_2 = \frac{P_2'}{2} Z^2 + C_3 Z + C_4 \, , \tag{13}$$

where the prime symbol corresponds to the partial derivative with respect to X, and where the coefficients C_j, with $j = 1, 2, 3, 4$, can be calculated by using the boundary conditions of Eqs. (5,6,7,8). Doing so, we obtain the velocity profiles:

$$U_1 = P_1' \left\{ \frac{Z^2 - H_1^2}{2M} + \frac{Z + H_1}{M(\Delta - H_2) - (\Delta + H_1)} \left[\frac{\Delta^2 - H_1^2}{2M} - \Delta(\Delta - H_2) \right] \right\} \tag{14}$$
$$+ P_2' \left\{ \frac{(Z + H_1)(\Delta - H_2)^2}{2\left[M(\Delta - H_2) - (\Delta + H_1)\right]} \right\} - \frac{(V_1 + V_2)(Z + H_1)}{M(\Delta - H_2) - (\Delta + H_1)} - V_1 \, ,$$

$$U_2 = -P_1' \left\{ \frac{(Z - H_2)(\Delta + H_1)^2}{2(M(\Delta - H_2) - (\Delta + H_1))} \right\} + P_2' \left\{ \frac{Z^2 - H_2^2}{2} + (Z - H_2)\left[-\Delta + \frac{M(\Delta - H_2)^2}{2[M(\Delta - H_2) - (\Delta + H_1)]} \right] \right\} \tag{15}$$
$$- \frac{M(V_1 + V_2)(Z - H_2)}{M(\Delta - H_2) - (\Delta + H_1)} + V_2 \, ,$$

where $V_i = a_i \omega_i / c$. We then calculate the flow rates within the two fluid films, as:

$$Q_1 = \int_{-H_1}^{\Delta} U_1 dZ = -P_1' \frac{(\Delta + H_1)^3}{12M} \frac{4M(\Delta - H_2) - (\Delta + H_1)}{M(\Delta - H_2) - (\Delta + H_1)} + \frac{P_2'(H_1 + \Delta)^2 (H_2 - \Delta)^2}{4\left[M(\Delta - H_2) - (\Delta + H_1)\right]}$$
$$- V_1(\Delta + H_1) - \frac{(\Delta + H_1)^2 (V_1 + V_2)}{2\left[M(\Delta - H_2) - (\Delta + H_1)\right]} \, , \tag{16}$$

$$Q_2 = \int_{\Delta}^{H_2} U_2 \mathrm{d}Z = \frac{P_1'}{4} \frac{(\Delta - H_2)^2 (\Delta + H_1)^2}{[M(\Delta - H_2) - (\Delta + H_1)]} - P_2' \frac{(H_2 - \Delta)^3}{12} \frac{M(\Delta - H_2) - 4(\Delta + H_1)}{M(\Delta - H_2) - (\Delta + H_1)}$$
$$+ V_2(H_2 - \Delta) + \frac{M(\Delta - H_2)^2 (V_1 + V_2)}{2[M(\Delta - H_2) - (\Delta + H_1)]} , \quad (17)$$

which, by introducing ad-hoc auxiliary functions F_i and I_i, can be rewritten in a more compact fashion, as:

$$Q_1 = F_1(H_1, H_2, \Delta)P_1' + F_2(H_1, H_2, \Delta)P_2' + I_1(H_1, H_2, \Delta) , \quad (18)$$
$$Q_2 = F_3(H_1, H_2, \Delta)P_1' + F_4(H_1, H_2, \Delta)P_2' + I_2(H_1, H_2, \Delta) . \quad (19)$$

The thin-film equations for this system can be derived by invoking volume conservation in the two fluid layers, as:

$$\frac{\partial \Delta}{\partial T} + Q_1' = 0 , \quad (20)$$

$$\frac{\partial \Delta}{\partial T} - Q_2' = 0 . \quad (21)$$

Finally, Eq. (9) reads in dimensionless form:

$$\Delta'' - \mathrm{Bo}\Delta = \kappa (P_2 - P_1) , \quad (22)$$

where $\mathrm{Bo} = (l/l_\mathrm{c})^2$ denotes the Bond number of the problem which compares the relevant dynamical horizontal length scale l to the capillary length $l_\mathrm{c} = \sqrt{\sigma/[g(\rho_1 - \rho_2)]})$. The dimensionless compliance of the fluid interface is denoted by $\kappa = \mathrm{Ca}/\epsilon^3$, where $\mathrm{Ca} = \eta_2 c/\sigma$ is a capillary number and $\epsilon = d_2/l$ is a small lubrication parameter. The problem has three unknown fields: Δ, P_1 and P_2. These obey the set of three coupled differential equations given by Eqs. (20-22), together with the following spatial boundary conditions: $P_i \to 0$ and $\Delta \to 0$ at $X \to \pm\infty$.

III. PERTURBATION ANALYSIS

Following the approach of previous soft-lubrication studies [24, 26, 28, 30, 57], we assume that $\kappa \ll 1$ and perform an expansion of the fields up to first order in κ, as:

$$\Delta \simeq 0 + \kappa\Delta_1 , \quad (23)$$
$$P_1 \simeq P_{10} + \kappa P_{11} , \quad (24)$$
$$P_2 \simeq P_{20} + \kappa P_{21} , \quad (25)$$
$$U_1 \simeq U_{10} + \kappa U_{11} , \quad (26)$$
$$U_2 \simeq U_{20} + \kappa U_{21} , \quad (27)$$

where $\kappa\Delta_1$ is the deformation profile of the fluid interface at first order in κ, $\kappa^j P_{ij}$ the excess pressure field in layer i at perturbation order j, and $\kappa^j U_{ij}$ the velocity field in layer i at perturbation order j. Given the respective symmetries of the fields at each order in κ, it is more convenient to focus only on the $X > 0$ domain, and impose the following equivalent spatial boundary conditions: $P_{i0} = 0$, $P_{i1}' = 0$ and $\Delta_1 = 0$ at $X = 0$, as well as $P_{ij} \to 0$ and $\Delta_1 \to 0$ at $X \to +\infty$.

A. Zeroth-order solution

At zeroth order in κ, the fluid interface is undeformed. Equations (20,21) then lead to the following coupled ordinary differential equations for the two pressure fields:

$$F_{10}P_{10}' + F_{20}P_{20}' = k_1 - I_{10} , \quad (28)$$
$$F_{30}P_{10}' + F_{40}P_{20}' = k_2 - I_{20} , \quad (29)$$

where the k_i are integration constants, and where we have evaluated the above auxiliary functions at zeroth order in κ, as:

$$F_{10} = -\frac{H_1^3}{12M} \frac{4MH_2 + H_1}{MH_2 + H_1} , \qquad F_{20} = F_{30} = -\frac{H_1^2 H_2^2}{4(MH_2 + H_1)} , \qquad F_{40} = -\frac{H_2^3}{12} \frac{MH_2 + 4H_1}{MH_2 + H_1} , \quad (30)$$

$$I_{10} = \frac{H_1^2(V_1 + V_2)}{2(MH_2 + H_1)} - V_1 H_1 \ , \qquad I_{20} = V_2 H_2 - \frac{MH_2^2(V_1 + V_2)}{2(MH_2 + H_1)} \ . \tag{31}$$

The derivatives of the pressure fields can then be evaluated from the above expressions, to give:

$$P'_{10} = \frac{F_{40}(k_1 - I_{10}) - F_{20}(k_2 - I_{20})}{F_{10}F_{40} - F_{20}F_{30}} \ , \tag{32}$$

$$P'_{20} = \frac{F_{10}(k_2 - I_{20}) - F_{30}(k_1 - I_{10})}{F_{10}F_{40} - F_{20}F_{30}} \ . \tag{33}$$

The latter equations can be integrated, *e.g.* with Mathematica or an explicit finite-difference numerical method – both giving identical results. The obtained solutions will be analyzed in the discussion section.

B. First-order solution

According to Eq. (22), the zeroth-order pressure fields calculated above lead to a deflection of the interface at first order in κ, which satisfies:

$$\Delta_1'' - \mathrm{Bo}\Delta_1 = P_{20} - P_{10} \ . \tag{34}$$

The formal solution of Eq. (34) satisfying the above boundary conditions reads:

$$\Delta_1(X, T) = \Delta_c(T) \sinh\left(X\sqrt{\mathrm{Bo}}\right) - \frac{1}{\sqrt{\mathrm{Bo}}} \int_0^X \mathrm{d}Y \ [P_{20}(Y, T) - P_{10}(Y, T)] \sinh\left[(Y - X)\sqrt{\mathrm{Bo}}\right] \ , \tag{35}$$

where $\Delta_c(T) = \left(1/\sqrt{\mathrm{Bo}}\right) \int_0^\infty \mathrm{d}Y \ [P_{10}(Y, T) - P_{20}(Y, T)] \exp\left(-Y\sqrt{\mathrm{Bo}}\right)$. This solution can be numerically evaluated for fixed parameters Bo, M, α and β.

Then, from the obtained deflection at first order in κ, one can calculate the pressure fields at first order in κ, as explained hereafter. To begin with, the auxiliary functions are evaluated at first order in κ, as:

$$F_n \simeq F_{n0} + \kappa\Delta_1 \frac{\partial F_n}{\partial \Delta}\bigg|_{\Delta=0} \ , \tag{36}$$

$$I_m \simeq I_{m0} + \kappa\Delta_1 \frac{\partial I_m}{\partial \Delta}\bigg|_{\Delta=0} \ , \tag{37}$$

for $n = 1, 2, 3, 4$ and $m = 1, 2$. Introducing $G_{n0} = \frac{\partial F_n}{\partial \Delta}\big|_{\Delta=0}$, and $E_{m0} = \frac{\partial I_m}{\partial \Delta}\big|_{\Delta=0}$, and expending the fluxes as $Q_i \simeq Q_{i0} + \kappa Q_{i1}$, one gets the first-order corrections to the fluxes:

$$Q_{11} \simeq F_{10}P'_{11} + \Delta_1 G_{10}P'_{10} + F_{20}P'_{21} + \Delta_1 G_{20}P'_{20} + \Delta_1 E_{10} \ , \tag{38}$$
$$Q_{21} \simeq F_{30}P'_{11} + \Delta_1 G_{30}P'_{10} + F_{40}P'_{21} + \Delta_1 G_{40}P'_{20} + \Delta_1 E_{20} \ . \tag{39}$$

Furthermore, the thin-film equations and the $X = 0$ boundary conditions imply:

$$Q_{11} = -\int_0^X \frac{\partial \Delta_1}{\partial T}\mathrm{d}X \ , \tag{40}$$

$$Q_{21} = \int_0^X \frac{\partial \Delta_1}{\partial T}\mathrm{d}X \ . \tag{41}$$

Combining the last four equations leads to:

$$F_{10}P'_{11} + F_{20}P'_{21} = -\mathcal{K} - \mathcal{J}_1 \ , \tag{42}$$
$$F_{30}P'_{11} + F_{40}P'_{21} = \mathcal{K} - \mathcal{J}_2 \ , \tag{43}$$

with:

$$\mathcal{J}_1 = \Delta_1 (G_{10}P'_{10} + G_{20}P'_{20} + E_{10}) \ , \tag{44}$$
$$\mathcal{J}_2 = \Delta_1 (G_{30}P'_{10} + G_{40}P'_{20} + E_{20}) \ , \tag{45}$$
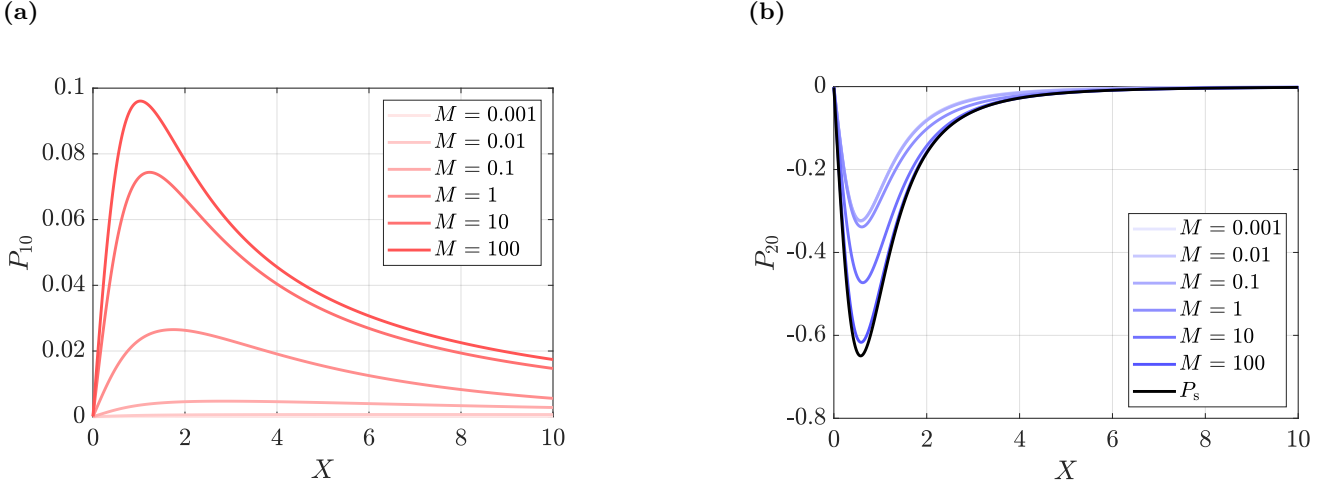$$\mathcal{K} = \int_0^X \frac{\partial \Delta_1}{\partial T}\mathrm{d}X \ . \tag{46}$$

(a)

(b)

FIG. 2: **Zeroth-order excess pressure fields,** P_{10} **(a) and** P_{20} **(b), as functions of the horizontal coordinate** X**, as evaluated from Eqs. (32,33) for** $\alpha = 15$ **and** $\beta = 99$**, with** $V_1 = 1$ **and** $V_2 = 1$**, and different values of** M **as indicated. The black line in panel (b) represents the pressure profile** P_s **generated near a solid boundary [10].**

Decoupling the equations, leads to:

$$P'_{11} = \frac{F_{40}\mathcal{H}_1 - F_{20}\mathcal{H}_2}{F_{10}F_{40} - F_{20}F_{30}} \; , \tag{47}$$

$$P'_{21} = \frac{F_{10}\mathcal{H}_2 - F_{30}\mathcal{H}_1}{F_{10}F_{40} - F_{20}F_{30}} \; , \tag{48}$$

with $\mathcal{H}_1 = -\mathcal{K} - \mathcal{J}_1$ and $\mathcal{H}_2 = \mathcal{K} - \mathcal{J}_2$. These can be numerically integrated over X, for fixed parameters Bo, M, α and β, using the far-field boundary conditions. The obtained solutions will be analyzed in the discussion section.

We conclude this section by an important remark. In the above expressions, we see that $\mathcal{K}$ involves the accelerations of the cylinders, while $\mathcal{J}_1$ and $\mathcal{J}_2$ both involve squared velocities instead. Moreover, the first-order corrections of the pressure fields are linear combinations of $\mathcal{K}$ and $\mathcal{J}_i$, which is reminiscent of past soft-lubrication studies [38, 58, 59]. Therefore, in order to address these two independent forcing modes later on, we split $\mathcal{H}_1$ and $\mathcal{H}_2$ into their: i) squared-velocity-dependant contributions $(\mathcal{H}_i)_{U^2}$, generically denoted by the subscript "U^2", and referred to as "lift" terms ; and ii) acceleration-dependant contributions $(\mathcal{H}_i)_{\dot{U}}$, generically denoted by the subscript "$\dot{U}$", and referred to as "inertial" terms. These contributions read:

$$(\mathcal{H}_1)_{U^2} = -\mathcal{J}_1 \; , \tag{49}$$

$$(\mathcal{H}_2)_{U^2} = -\mathcal{J}_2 \; , \tag{50}$$

$$(\mathcal{H}_1)_{\dot{U}} = -\mathcal{K} \; , \tag{51}$$

$$(\mathcal{H}_2)_{\dot{U}} = \mathcal{K} \; . \tag{52}$$

IV. DISCUSSION

Hereafter, keeping $\beta \gg 1$ in order to approach the situation of a cylinder moving near a thin, supported and flat fluid film, we discuss the zeroth-order and first-order solutions, and investigate the influence of the three other key dimensionless parameters of the problem: the viscosity ratio M, the gap ratio α, and the Bond number Bo.

A. Zeroth-order pressure

The zeroth-order excess pressure fields in the two layers are computed from Eqs. (32,33) and plotted in Fig. 2, for $\alpha = 15$ and $\beta = 99$, and for different values of the viscosity ratio M. For comparison, we also show the pressure $P_s(X) = -2V_2 X/(1 + X^2)^2$ [10] generated if the fluid interface was replaced by a no-slip solid boundary. The pressure fields in both layers appear to have opposite signs. Furthermore, due to the allowed flow in the bottom layer, the pressure generated in the top layer is lower than if the interface was a no-slip solid substrate. However, increasing
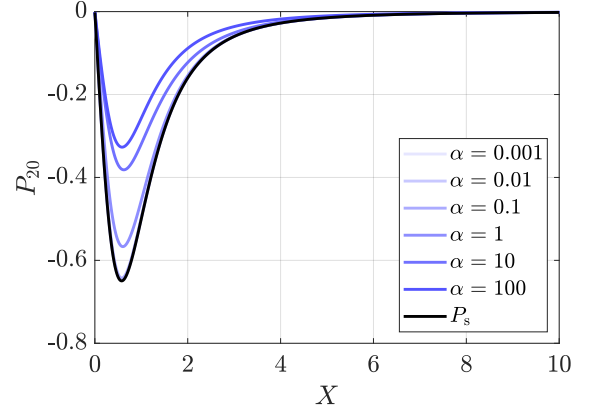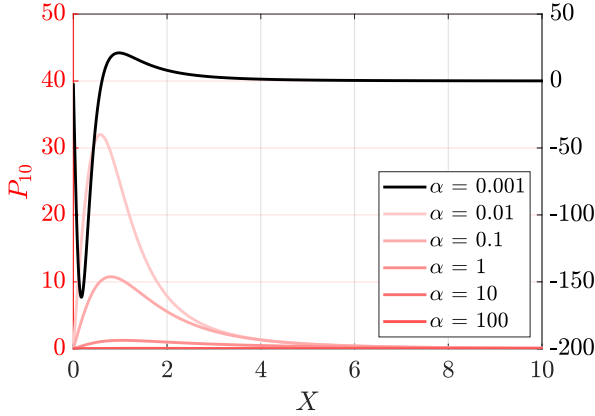
(a)

FIG. 3: Zeroth-order excess pressure fields, P_{10} (a) and P_{20} (b), as functions of the horizontal coordinate X, as evaluated from Eqs. (32,33) for $M = 2$ and $\beta = 99$, with $V_1 = 1$ and $V_2 = 1$, and different values of α as indicated. The black line in panel (a) represents the top-layer pressure field for $\alpha = 0.001$, with the appropriate scale on the right y-axis. The black line in panel (b) represents the pressure profile $P_{\rm s}$ generated near a solid boundary [10].

M, $i.e.$ increasing the viscosity of the bottom layer with respect to the one in the top layer increases the pressure magnitude in both layers. Eventually, at large M, the pressure field in the top layer saturates towards $P_{\rm s}$, as expected.

In Fig. 3, we investigate the effect of the ratio α between the bottom-layer and top-layer thicknesses. Reducing α increases the magnitude of the pressure generated in the top layer, as expected due to the reducing flow ability in the bottom layer. Once again, the curves eventually saturate towards the no-slip solid pressure $P_{\rm s}$. Interestingly, at some point, the decrease of α leads to a sign change for the bottom-layer pressure. The transition point of such a sign change depends (not shown) upon the chosen values of M and β.

B. Interface deflection

The first-order interface deflection field is calculated using Eq. (35) and plotted in Fig. 4 for several Bo values. While the horizontal range and the magnitude are both affected by Bo, the former can be absorbed into a rescaled horizontal coordinate $X\sqrt{\rm Bo}$. This is characteristic of problems involving capillarity and a direct consequence of the Young-Laplace condition of Eq. (34). Besides, the deflection magnitude decreases as Bo is increased, since gravitational resistance towards interface deformation is increased. However, the decrease does not seem to follow a simple scaling law with Bo.

Let us now investigate the influence of the viscosity ratio M and gap ratio α. The results are plotted in Fig. 5. As M increases, the zeroth-order pressure fields increase in magnitude monotonically, leading to a corresponding increase in the magnitude of the interface deflection. Similarly, decreasing α increases the magnitude of the interface deflection. However, the sign change for the bottom-layer pressure field observed previously at small α leads to an intricate behaviour of the interface deflection profile. Further decreasing (not shown) α can even lead to a complete sign flip of the interface deflection.

C. First-order pressure

Integrating Eqs. (47,48) allows us to find the first-order pressure corrections $P_{i1} = {}_{U^2}P_{i1} + {}_{\dot{U}}P_{i1}$, which are separated into two different contributions as mentioned beforehand: i) lift terms ${}_{U^2}P_{i1}$; and ii) inertial terms ${}_{\dot{U}}P_{i1}$. We further stress that our discussion below focuses only on the top layer, as our goal is to eventually calculate the force generated on the top cylinder. The lift and inertial terms in the top layer are shown in Fig. 6 for a given set of parameters. As we see, they typically push the cylinder away from the interface. Besides, as the Bond number Bo is increased, one observes (not shown) a decrease in both the lift and inertial terms, which is due to the reducing interface deflection observed above.

Moreover, the effects of the viscosity ratio M and gap ratio α are presented in Figs. 7 and 8. Increasing M, or
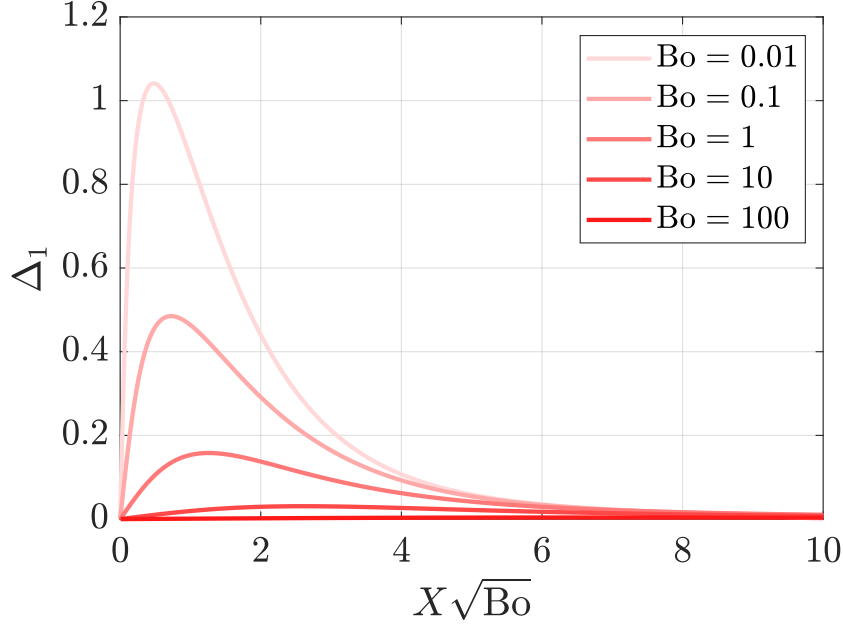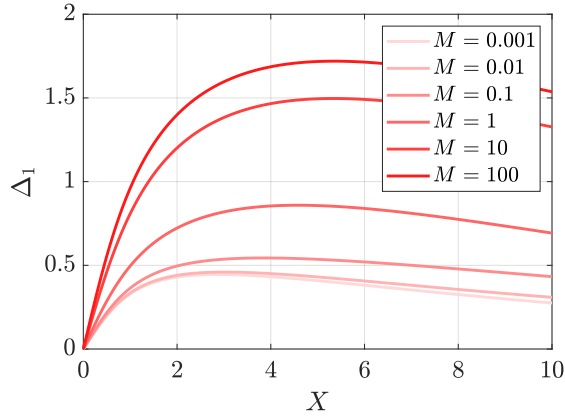
FIG. 4: **First-order interface deflection profile** Δ_1 **as a function of rescaled horizontal coordinate** $X\sqrt{\mathrm{Bo}}$, **as calculated from Eq. (35) with** $M = 2$, $\alpha = 15$, $\beta = 99$, $V_1 = 0$, $V_2 = 1$, **and for several Bo values as indicated.**
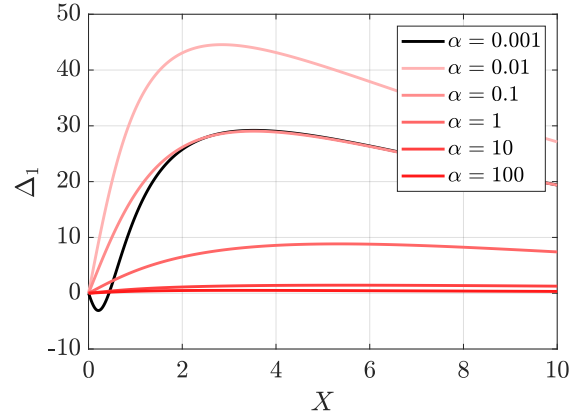
(a)   **(b)**

FIG. 5: **First-order interface deflection profile** Δ_1 **as a function of horizontal coordinate** X, **as calculated from Eq. (35) with Bo** $= 0.01$, $\beta = 99$, $V_1 = 0$ **and** $V_2 = 1$, **for: (a)** $\alpha = 15$ **and varying** M **as indicated; and (b)** $M = 2$ **and varying** α **as indicated.**

decreasing α, increases the magnitude of both the lift and inertial terms. This is explained once again by the reducing flow ability in the bottom layer. However, interestingly, for very small α values, where the zeroth-order pressure field in the bottom layer changes sign, the first-order pressure field in the top layer reduces in magnitude.

D. Capillary-lubrication force

In dimensional units, the normal force per unit length F felt by the top cylinder can be found by integrating the pressure field p_2 in the top layer along the horizontal coordinate x. At zeroth order, the force is null by symmetry of
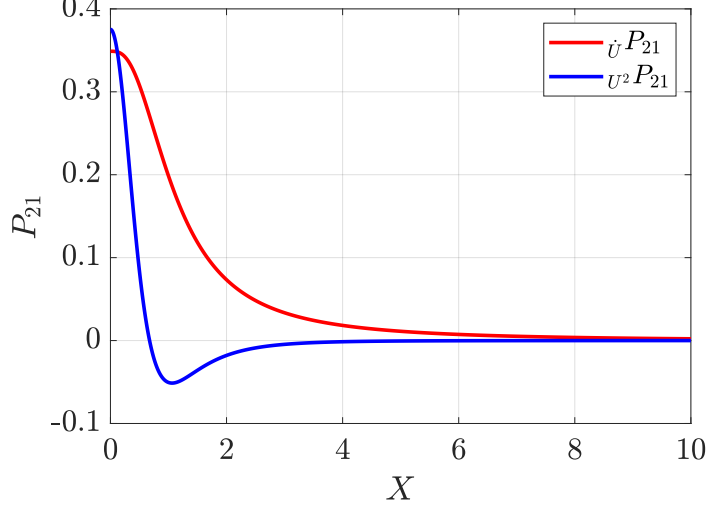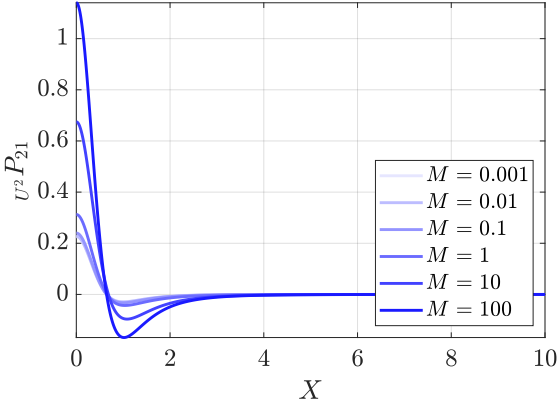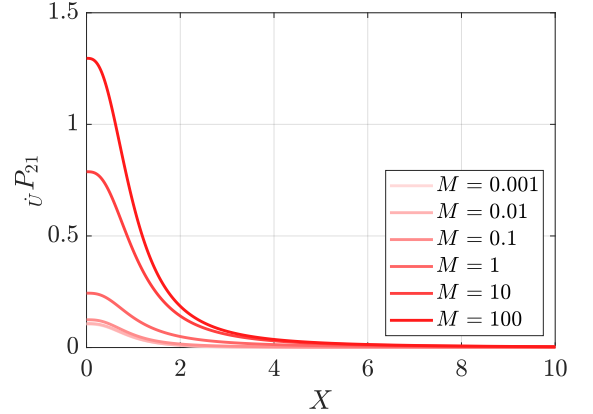
FIG. 6: **First-order pressure correction** P_{21} **in the top layer as a function of horizontal coordinate** X**, as obtained from numerically solving Eqs. (47,48) for** $M = 2$**,** $\alpha = 15$**,** $\beta = 99$**, and Bo $= 0.01$. Both the lift term** $_{U^2}P_{21}$ **(blue) for** $V_1 = 0$ **and** $V_2 = 1$**, and inertial term** $_{\dot{U}}P_{21}$ **(red) for** $\dot{V}_1 = 0$ **and** $\dot{V}_2 = 1$**, are shown.**

(a)   **(b)**

FIG. 7: **First-order pressure correction** P_{21} **in the top layer as a function of horizontal coordinate** X**, as obtained from numerically solving Eqs. (47,48) with** $\alpha = 15$**,** $\beta = 99$**, and Bo $= 0.01$, and for various** M **as indicated. Both the lift term** $_{U^2}P_{21}$ **(a) with** $V_1 = 0$ **and** $V_2 = 1$**, and inertial term** $_{\dot{U}}P_{21}$ **(b) with** $\dot{V}_1 = 0$ **and** $\dot{V}_2 = 1$**, are shown.**

the excess pressure fields. At leading order in perturbation, one thus has:

$$F = \int_{-\infty}^{\infty} p_2 \mathrm{d}x \simeq \frac{\eta_2^2 \omega_2^2 a_2^2}{\sigma} \left(\frac{a_2}{d_2}\right)^{5/2} {}_{U^2}\psi_{21} + \frac{\eta_2^2 \dot{\omega}_2 a_2^2}{\sigma} \left(\frac{a_2}{d_2}\right)^2 {}_{\dot{U}}\psi_{21} \ , \tag{53}$$

where $_{U^2}\psi_{21} = (2^{7/2}/V_2^2) \int_0^{\infty} {}_{U^2}P_{21}\mathrm{d}X$ and $_{\dot{U}}\psi_{21} = (2^4/\dot{V}_2) \int_0^{\infty} {}_{\dot{U}}P_{21}$ are dimensionless coefficients corresponding to the lift and inertial terms, respectively. These two coefficients are plotted in Fig. 9 as functions of the viscosity ratio M and for various gap ratios α. Two main comments can be made on the results. First, the coefficients vary by orders of magnitude upon changing the two ratios, which indicates the possibility of tuning the conditions to modify, control and optimize the capillary-lubrication effects. Moreover, in direct contrast to classical elastic soft lubrication [39], the coefficients signs can be changed too, as already reported for the lift force in a recent study on viscoelastic fluid substrates [54].

    We saw earlier that increasing Bo reduces the deflection of the interface and in turn the first-order pressures. The variation of the lift coefficient $_{U^2}\psi_{21}$ is thus plotted in Fig. 10 against Bo and for different values of α. For
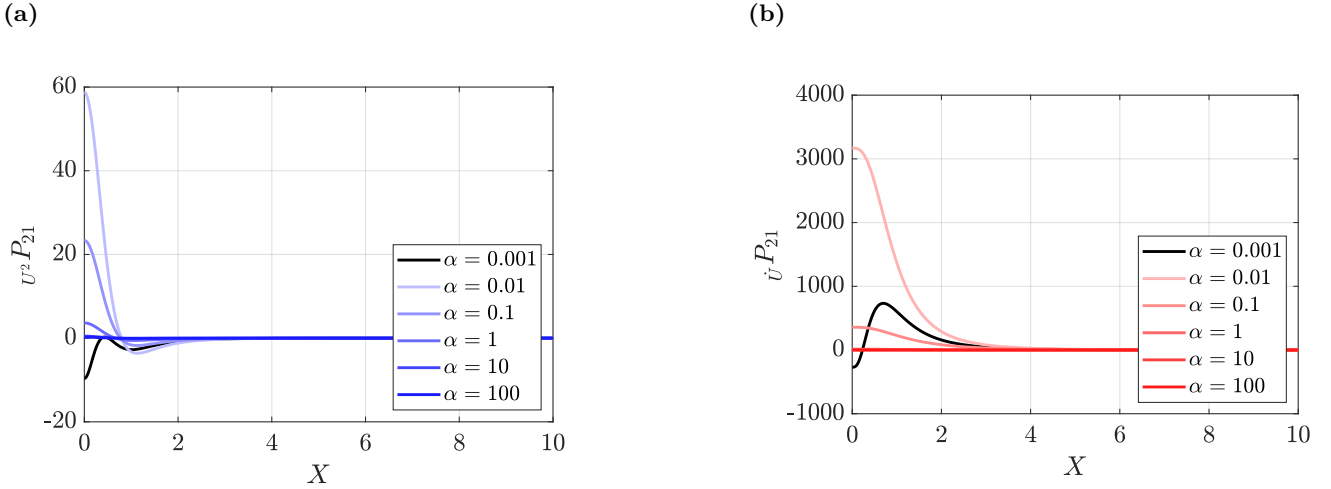
(a)

(b)

FIG. 8: First-order pressure correction P_{21} in the top layer as a function of horizontal coordinate X, as obtained from numerically solving Eqs. (47,48) with $M = 2$, $\beta = 99$, and Bo $= 0.01$, and for various α as indicated. Both the lift term $_{U^2}P_{21}$ (a) with $V_1 = 0$ and $V_2 = 1$, and inertial term $_{\dot{U}}P_{21}$ (b) with $\dot{V}_1 = 0$ and $\dot{V}_2 = 1$, are shown.
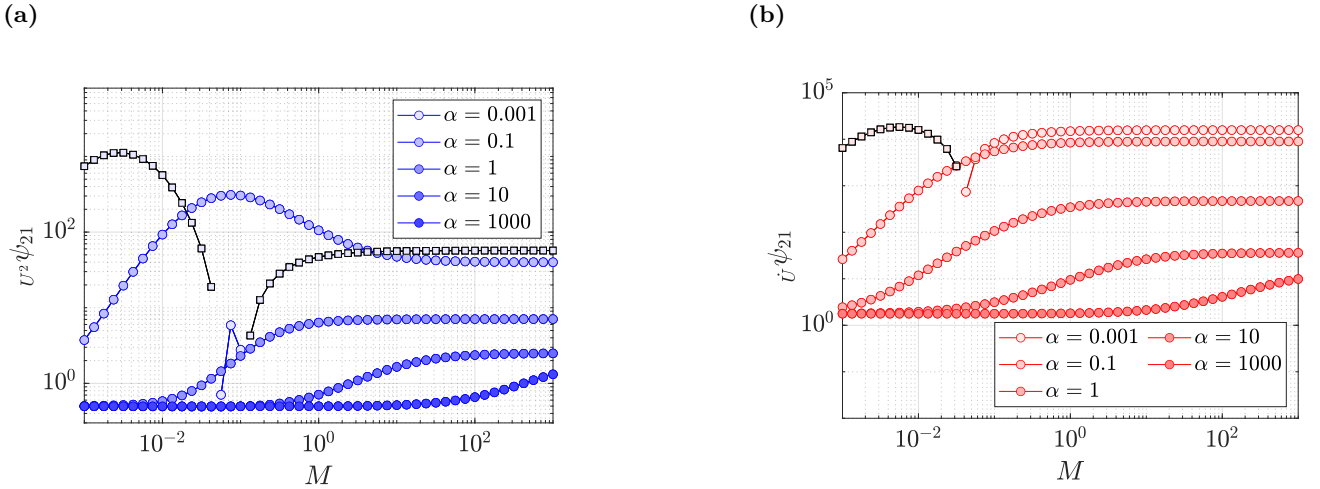
(a)

(b)

FIG. 9: Lift coefficient $_{U^2}\psi_{21}$ (a) and inertial coefficient $_{\dot{U}}\psi_{21}$ (b) of the first-order normal force per unit length (see Eq. (53)) exerted on the top cylinder as functions of the viscosity ratio M and for various gap ratios α. These coefficients were obtained from numerical integration of P_{21} along X, as computed for Bo $= 0.01$, $\beta = 99$, and for either $V_1 = 0$, $V_2 = 1$ (a), or $\dot{V}_1 = 0$, $\dot{V}_2 = 1$ (b). The squares denote the absolute values in the case of negative values.

small Bo values, the decrease is affine. For large Bo values, the lift coefficient becomes inversely proportional to Bo. Interestingly, in the latter regime, the curvature term in Eq. (34) becomes negligible, and the interface response becomes Winkler-like [30]. However, it is to be remarked that, in contrast to pure Winkler solids, there are still flows in the bottom layer here.

Finally, in dimensional units, the torque per unit length T generated on the top cylinder is found by integrating the shear stress, as:

$$T = -a_2 \int_{-\infty}^{\infty} \eta_2 \frac{\partial u_2}{\partial z}\bigg|_{z=h_2} \mathrm{d}x \simeq -\eta_2 \omega_2 a_2^2 \left(\frac{a_2}{d_2}\right)^{1/2} \phi_{20} \ , \tag{54}$$

with $\phi_{20} = (2^{3/2}/V_2) \int_0^{\infty} \frac{\partial U_{20}}{\partial Z}\big|_{Z=H_2} \mathrm{d}X$ the zeroth-order dimensionless coefficient. Indeed, by symmetry of the velocity field, there is no contribution at first order in compliance. The zeroth-order coefficient ϕ_{20} is plotted in Fig. 11 against the viscosity ratio M, and for different values of the gap ratio α. We first see that for all α the zeroth-order coefficient saturates to two limiting values, for $M \to 0$ and $M \to \infty$ respectively. The latter corresponds
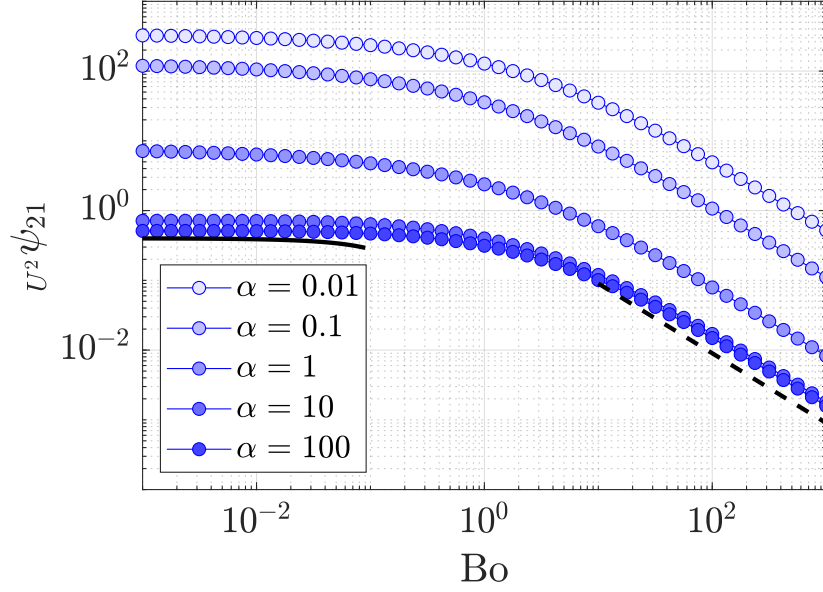
FIG. 10: Lift coefficient $_{U^2}\psi_{21}$ of the first-order normal force per unit length (see Eq. (53)) exerted on the top cylinder as a function of the Bond number Bo and for various gap ratios α. This coefficient was obtained from numerical integration of P_{21} along X, as computed for $M = 1$, $\beta = 99$, $V_1 = 0$, and $V_2 = 1$. The solid line corresponds to an affine decrease with Bo, while the dashed line corresponds to a $\sim 1/$Bo power law.
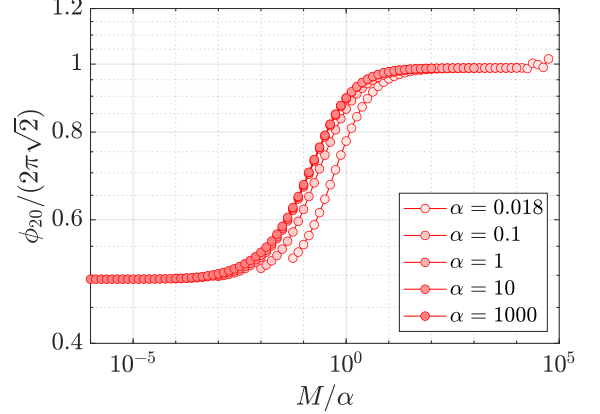
(a)
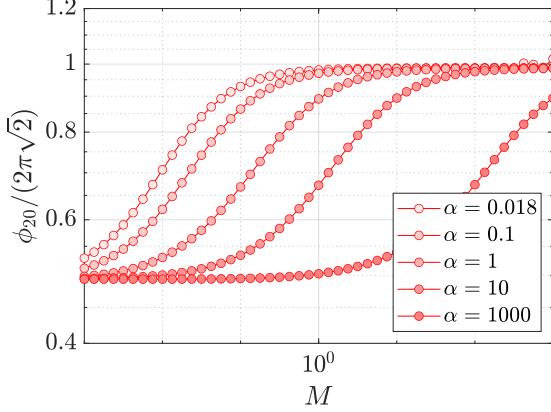
(b)

FIG. 11: (a) Coefficient ϕ_{20} of the zeroth-order torque per unit length (see Eq. (??)) exerted on the top cylinder, and normalized by the value for a rigid no-slip boundary, as a function of the viscosity ratio M and for various gap ratios α. This coefficient was computed for $\beta = 99$, $V_1 = 0$, and $V_2 = 1$. (b) Same data with a rescaled parameter M/α on the x-axis.

to the no-slip rigid case, as expected. Moreover, inspired by our previous study on the normal motion [59], we observe a collapse when using the rescaled parameter M/α, for $\alpha > 1$.

V. CONCLUSION

We have studied two rotating cylinders separated by a capillary interface in between two lubricating viscous films. Specifically, by using a perturbative expansion in the limit of small deformation of the interface, we have numerically calculated the pressure fields, the interface deflection, and the subsequent force generated on one cylinder. These

were separated into lift and inertial-like contributions. We have further investigated the influence of all the relevant geometrical and physical parameters of the problem on these contributions and have revealed a large degree of tunability of their magnitudes and even signs. The latter peculiar feature is absent of classical elastic soft lubrication and highlights the interest of such capillary-lubrication settings. Our results pave the way towards the characterization of colloidal mobility near complex boundaries.

ACKNOWLEDGMENTS

[1] H. Lamb, *Hydrodynamics* (University Press, 1924).

[2] G. K. Batchelor, *An Introduction to Fluid Dynamics* (Cambridge University Press, 1967).

[3] G. Jeffery, On the steady rotation of a solid of revolution in a viscous fluid, Proceedings of the London Mathemathical Society **2**, 327 (1915).

[4] W. Collins, On the steady rotation of a sphere in a viscous fluid, Mathematika **2**, 42 (1955).

[5] W. Dean and M. O'Neill, A slow motion of viscous liquid caused by the rotation of a solid sphere, Mathematika **10**, 13 (1963).

[6] M. E. O'Neill, A slow motion of viscous liquid caused by a slowly moving solid sphere, Mathematika **11**, 67 (1964).

[7] M. O'Neill and K. Stewartson, On the slow motion of a sphere parallel to a nearby plane wall, Journal of Fluid Mechanics **27**, 705 (1967).

[8] A. J. Goldman, R. G. Cox, and H. Brenner, Slow viscous motion of a sphere parallel to a plane wall—i motion through a quiescent fluid, Chemical engineering science **22**, 637 (1967).

[9] M. Cooley and M. O'Neill, On the slow motion generated in a viscous fluid by the approach of a sphere to a plane wall or stationary sphere, Mathematika **16**, 37 (1969).

[10] D. Jeffrey and Y. Onishi, The slow motion of a cylinder next to a plane wall, The Quarterly Journal of Mechanics and Applied Mathematics **34**, 129 (1981).

[11] B. J. Hamrock, S. R. Schmid, and B. O. Jacobson, *Fundamentals of fluid film lubrication* (CRC press, 2004).

[12] J. Hou, V. C. Mow, W. Lai, and M. Holmes, An analysis of the squeeze-film lubrication mechanism for articular cartilage, Journal of biomechanics **25**, 247 (1992).

[13] M. Hlaváček, The role of synovial fluid filtration by cartilage in lubrication of synovial joints—i. mixture model of synovial fluid, Journal of biomechanics **26**, 1145 (1993).

[14] M. Abkarian, C. Lartigue, and A. Viallat, Tank treading and unbinding of deformable vesicles in shear flow: determination of the lift force, Physical review letters **88**, 068103 (2002).

[15] J. Happel and H. Brenner, *Low Reynolds number hydrodynamics: with special applications to particulate media*, Vol. 1 (Springer Science & Business Media, 1983).

[16] G. Batchelor, The stress system in a suspension of force-free particles, Journal of fluid mechanics **41**, 545 (1970).

[17] G. Batchelor, The stress generated in a non-dilute suspension of elongated particles by pure straining motion, Journal of Fluid Mechanics **46**, 813 (1971).

[18] G. Batchelor, Brownian diffusion of particles with hydrodynamic interaction, Journal of Fluid Mechanics **74**, 1 (1976).

[19] G. Batchelor, The effect of brownian motion on the bulk stress in a suspension of spherical particles, Journal of fluid mechanics **83**, 97 (1977).

[20] S. Leroy and E. Charlaix, Hydrodynamic interactions for the measurement of thin film elastic properties, Journal of Fluid Mechanics **674**, 389 (2011).

[21] S. Leroy, A. Steinberger, C. Cottin-Bizonne, F. Restagno, L. Léger, and E. Charlaix, Hydrodynamic interaction between a spherical particle and an elastic surface: a gentle probe for soft thin films, Physical review letters **108**, 264501 (2012).

[22] L. Garcia, C. Barraud, C. Picard, J. Giraud, E. Charlaix, and B. Cross, A micro-nano-rheometer for the mechanics of soft matter at interfaces, Review of Scientific Instruments **87**, 113906 (2016).

[23] F. Basoli, S. M. Giannitelli, M. Gori, P. Mozetic, A. Bonfanti, M. Trombetta, and A. Rainer, Biomechanical characterization at the cell scale: present and prospects, Frontiers Physiol. **9**, 1449 (2018).

[24] K. Sekimoto and L. Leibler, A mechanism for shear thickening of polymer-bearing surfaces: elasto-hydrodynamic coupling, Europhysics Letters **23**, 113 (1993).

[25] J. Beaucourt, T. Biben, and C. Misbah, Optimal lift force on vesicles near a compressible substrate, Europhys. Lett. **67**, 676 (2004).

[26] J. Skotheim and L. Mahadevan, Soft lubrication: The elastohydrodynamics of nonconforming and conforming contacts, Physics of Fluids **17**, 092101 (2005).

[27] S. J. Weekley, S. L. Waters, and O. E. Jensen, Transient elastohydrodynamic drag on a particle moving near a deformable wall, Q. J. Mech. Appl. Math. **59**, 277 (2006).

[28] J. Urzay, S. G. Llewellyn Smith, and B. J. Glover, The elastohydrodynamic force on a sphere near a soft wall, Physics of Fluids **19**, 103106 (2007).

[29] J. H. Snoeijer, J. Eggers, and C. H. Venner, Similarity theory of lubricated hertzian contacts, Phys. Fluids **25**, 101705 (2013).

[30] T. Salez and L. Mahadevan, Elastohydrodynamics of a sliding, spinning and sedimenting cylinder near a soft wall, Journal of Fluid Mechanics **779**, 181 (2015).

[31] A.-S. Bouchet, C. Cazeneuve, N. Baghdadli, G. S. Luengo, and C. Drummond, Experimental study and modeling of boundary lubricant polyelectrolyte films, Macromolecules **48**, 2244 (2015).

[32] B. Saintyves, T. Jules, T. Salez, and L. Mahadevan, Self-sustained lift and low friction via soft lubrication, Proc. Nat. Acad. Sci. **113**, 5847 (2016).

[33] H. S. Davies, D. Debarre, N. El Amri, C. Verdier, R. P. Richter, and L. Bureau, Elastohydrodynamic lift at a soft wall, Phys. Rev. Lett. **120**, 198001 (2018).

[34] B. Rallabandi, N. Oppenheimer, M. Y. B. Zion, and H. A. Stone, Membrane-induced hydroelastic migration of a particle surfing its own wave, Nature Phys. **14**, 1211 (2018).

[35] P. Vialar, P. Merzeau, S. Giasson, and C. Drummond, Compliant surfaces under shear: Elastohydrodynamic lift force, Langmuir **35**, 15605 (2019).

[36] Z. Zhang, V. Bertin, M. Arshad, E. Raphael, T. Salez, and A. Maali, Direct measurement of the elastohydrodynamic lift force at the nanoscale, Physical Review Letters **124**, 054502 (2020).

[37] M. H. Essink, A. Pandey, S. Karpitschka, C. H. Venner, and J. H. Snoeijer, Regimes of soft lubrication, J. Fluid Mech. **915** (2021).

[38] V. Bertin, Y. Amarouchene, E. Raphael, and T. Salez, Soft-lubrication interactions between a rigid sphere and an elastic wall, Journal of Fluid Mechanics **933**, A23 (2022).

[39] L. Bureau, G. Coupier, and T. Salez, Lift a low reynolds number, ArXiv **2207.04538** (2023).

[40] B. Rallabandi, Fluid-elastic interactions near contact at low reynolds number, Annual Review of Fluid Mechanics **56**, 491 (2024).

[41] N. J. Balmforth, C. J. Cawthorn, and R. V. Craster, Contact in a viscous fluid. part 2. a compressible fluid and an elastic solid, J. Fluid Mech. **646**, 339 (2010).

[42] R. Clarke and S. Potnis, Elastohydrodynamics induced by a rapidly moving microscopic body, Proceedings of the Royal Society A: Mathematical, Physical and Engineering Sciences **467**, 2852 (2011).

[43] A. Rinehart, U. Lācis, T. Salez, and S. Bagheri, Lift induced by slip inhomogeneities in lubricated contacts, Physical Review Fluids **5**, 082001 (2020).

[44] K. Aderogba and J. Blake, Action of a force near the planar surface between two semi-infinite immiscible liquids at very low reynolds numbers, Bulletin of the Australian Mathematical Society **18**, 345 (1978).

[45] S. Nezamipour and A. Najafi, Flow pumping by external periodic shear applied to a soft interface, Scientific Reports **11**, 15041 (2021).

[46] S. Lee, R. Chadwick, and L. G. Leal, Motion of a sphere in the presence of a plane interface. part 1. an approximate solution by generalization of the method of lorentz, Journal of Fluid Mechanics **93**, 705 (1979).

[47] S. Lee and L. Leal, Motion of a sphere in the presence of a plane interface. part 2. an exact solution in bipolar co-ordinates, Journal of Fluid Mechanics **98**, 193 (1980).

[48] S. Lee and L. Leal, The motion of a sphere in the presence of a deformable interface: Ii. a numerical study of the translation of a sphere normal to an interface, Journal of Colloid and Interface Science **87**, 81 (1982).

[49] A. Geller, S. Lee, and L. Leal, The creeping motion of a spherical particle normal to a deformable interface, Journal of Fluid Mechanics **169**, 27 (1986).

[50] S.-M. Yang and L. G. Leal, Particle motion in stokes flow near a plane fluid-fluid interface. part 1. slender body in a quiescent fluid, Journal of Fluid Mechanics **136**, 393 (1983).

[51] R. Trouilloud, S. Y. Tony, A. Hosoi, and E. Lauga, Soft swimming: Exploiting deformable interfaces for low reynolds number locomotion, Physical review letters **101**, 048102 (2008).

[52] D. Lopez and E. Lauga, Dynamics of swimming bacteria at complex interfaces, Physics of Fluids **26**, 400 (2014).

[53] N. Desai and A. M. Ardekani, Biofilms at interfaces: microbial distribution in floating films, Soft Matter **16**, 1731 (2020).

[54] S. Hu, F. Meng, *et al.*, Effect of fluid viscoelasticity, shear stress, and interface tension on the lift force in lubricated contacts, The Journal of Chemical Physics **159** (2023).

[55] O. Reynolds, On the theory of lubrication and its application to mr beauchamp tower's experiments, including an experimental determination of the viscosity of olive oil., Philos. Trans. R. Soc. Lond. **177**, 157 (1886).

[56] A. Oron, S. Davis, and S. Bankoff, Long-scale evolution of thin liquid films, Rev. Mod. Phys. **69**, 931 (1997).

[57] A. Pandey, S. Karpitschka, C. H. Venner, and J. H. Snoeijer, Lubrication of soft viscoelastic solids, Journal of fluid mechanics **799**, 433 (2016).

[58] F. Kaveh, J. Ally, M. Kappl, and H.-J. Butt, Hydrodynamic force between a sphere and a soft, elastic surface, Langmuir **30**, 11619 (2014).

[59] A. Jha, Y. Amarouchene, and T. Salez, Capillary-lubrication force exerted on a two-dimensional particle moving towards a thin fluid film, Journal of Fluid Mechanics **977**, A50 (2023).